Journal of Systematic Innovation 8[22]1-11: e4822111
Article

Influence of concentration, acid type and calcination temperature on TiO_2 synthesis

Influencia de la concentración, el tipo de ácido y la temperatura de calcinación en la síntesis de TiO_2

Del Ángel-Sánchez, María Magdalena [a] & Martínez-Carreón, María de Jesús *[b]

[a] Universidad Tecnológica Gral. Mariano Escobedo • LDG-8077-2024 • 0009-0002-9241-5117 • 416112
[b] Universidad Autónoma de Nuevo León • IYJ-9475-2023• 0000-0002-9283-7857 • 290939

CONAHCYT Classification:

Area: Physics-Mathematics and Earth Sciences
Field: Physics
Discipline: Physics of the solid state
Subdiscipline: Crystal structure

https://doi.org/10.35429/JSI.2024.8.22.1.11
History of the article:
Received: January 08, 2024
Accepted: December 04, 2024

* ✉ [maria.martinezcr@uanl.edu.mx]

Abstract

Titanium dioxide (TiO_2) is employed in various environmental science applications due to its exceptional photocatalytic activity and semiconductor behavior. The efficacy of TiO_2 in these applications is intrinsically linked to its crystal structure, morphology and particle size. Titanium dioxide exhibits three well-defined crystalline phases: Anatase (octahedral structure), Rutile (tetragonal structure) and Brookite (orthorhombic structure). This work studies the effect of different concentrations, types of acids, and calcination temperatures on the crystalline structure and morphology of TiO_2 synthesized via hydrothermal route using characterization techniques such as DLS (Dynamic Light Scattering), ATR-FTIR (Attenuated Total Reflectance Fourier Transform Infrared Spectroscopy), XRD (X-Ray Diffraction) and SEM (Scanning Electron Microscopy).

Influence of concentration, acid type and calcination temperature on TiO_2 synthesis

OBJECTIVE:
Study the effect of different concentrations, types of acids, and calcination temperature on the crystalline structure and morphology of TiO_2 via hydrothermal method; In Series I varying the percentage of nitric acid and in Series II varying the ratio of HCl:HNO_3

SERIES I METHODOLOGY:

REACTANT	SAMPLE				
	I-1	I-2	I-3	I-4	I-5
HNO_3	0M	1M	3M	1M	0.5M
Ti i$(PrO)_4$	0.15M	0.15M	0.15M	0.15M	0.15M
NaF	-	-	-	0.01M	-

SERIES II METHODOLOGY:

REACTANT	SAMPLE		
	II-1	II-2	II-3
HNO_3	0.5M	1M	1.5M
HCl	2.5M	2M	1.5M
Ti i$(PrO)_4$	0.15M	0.15M	0.15M

SERIES I RESULTS:

SERIES II RESULTS:

Titanium dioxide TiO_2, Hydrothermal synthesis, Structural analysis.

Resumen

El dióxido de titanio (TiO_2) se emplea en diversas aplicaciones de ciencia ambiental debido a su excepcional actividad fotocatalítica y su comportamiento como semiconductor, La eficacia del TiO_2 en estas aplicaciones está intrínsecamente ligada a su estructura cristalina, morfología y tamaño de partícula. El TiO_2 presenta tres fases cristalinas bien definidas: Anatasa (estructura octaédrica), Rutilo (estructura tetragonal) y Brookita (estructura ortorrómbica). En este trabajo se estudia el efecto de diferentes concentraciones, tipos de ácidos y temperatura de calcinación en la estructura cristalina y morfología del TiO_2 sintetizado por vía hidrotermal mediante las técnicas de caracterización de dispersión de luz dinámica (DLS), espectroscopia infrarroja por transformada de Fourier con reflectancia total atenuada (ATR-FTIR), difracción de rayos X (XRD) y microscopía electrónica de barrido (SEM).

Influencia de la concentración, el tipo de ácido y la temperatura de calcinación en la síntesis de TiO_2

OBJETIVO:
Estudiar el efecto de diferentes concentraciones, tipos de ácidos y temperatura de calcinación en la estructura cristalina y morfología del TiO_2 por vía hidrotermal; En la síntesis I variando el porcentaje de ácido nítrico y en la Serie II variando la relación de HCl:HNO_3

METODOLOGÍA SERIE I:

REACTIVO	MUESTRA				
	I-1	I-2	I-3	I-4	I-5
HNO_3	0M	1M	3M	1M	0.5M
Ti i$(PrO)_4$	0.15M	0.15M	0.15M	0.15M	0.15M
NaF	-	-	-	0.01M	-

METODOLOGÍA SERIE II:

REACTIVO	MUESTRA		
	II-1	II-2	II-3
HNO_3	0.5M	1M	1.5M
HCl	2.5M	2M	1.5M
Ti i$(PrO)_4$	0.15M	0.15M	0.15M

RESULTADOS SERIE I:

RESULTADOS SERIE II

Dióxido de titanio TiO_2, Síntesis hidrotermal, Análisis estructural

Citation: Del Ángel-Sánchez, María Magdalena & Martínez-Carreón, María de Jesús. [2024]. Influence of concentration, acid type and calcination temperature on TiO_2 synthesis. Journal of Systematic Innovation. 8[22]1-11: e4822111.

Introduction

Titania has a wide range of applications in environmental science due to its excellent catalytic, optical and electrical properties (Farooq, 2024). It is frequently used for the photodegradation of organic molecules, water purification, disinfection of wastewater, self-cleaning coatings for buildings in urban areas and in water splitting for hydrogen generation (Ali, 2018). Additionally, exhibits utility in air remediation systems, disinfection processes, and targeted organic transformations (Arun, 2023). These applications highlight the importance of TiO_2 in addressing environmental challenges and promoting sustainability (Pelaez, 2012).

Numerous methodologies have been developed for the synthesis of titanium dioxide, encompassing techniques such as hydrothermal synthesis (Hidalgo, 2007), metal-organic chemical vapor deposition (MOCVD) (Li, 2002), electrochemical approaches (Anandgaonker, 2019), sonochemical processes (Guo, 2011), and green synthesis routes (Dülger, 2024), among others.

Hydrothermal synthesis of TiO_2 nanoparticles was performed. This method typically involves the crystallization of TiO_2 from a precursor solution under high pressure and temperature conditions. The hydrothermal process can produce either rutile or anatase phase nanoparticles depending on the specific conditions and precursors used (Gupta, 2021), (Rehan, 2011). The influence of reactant concentration and acid type on the final properties of TiO_2 nanoparticles synthesized via hydrothermal methods is an important area of research for evaluating the impact of key reaction parameters on their crystallinity (Kignelman, 2021).

Precursor concentration is known to significantly impact the size, morphology, and crystallinity of the resulting nanostructures (Bindra, 2022), (Huang, 2012), these factors directly influence the catalytic efficiency and potential applications of TiO_2. Similarly, the type of acid employed dictates the etching behavior during synthesis, thereby affecting the final morphology and size of the nanostructures (Eaimsumang, 2020). A thorough understanding of these influences allows for the targeted design and optimization of TiO_2 for specific applications.

In the present investigation, the effects of nitric acid (HNO_3) concentration gradients and calcination temperature on the hydrothermal fabrication of titanium dioxide are elucidated. Furthermore, this work delineates the comparative impact of acid type on TiO_2 synthesis by utilizing both HNO_3 and hydrochloric acid (HCl) across a spectrum of concentrations and thermal conditions.

Materials and methods

Two series of syntheses were conducted. In series I, different concentrations of nitric acid and two distinct calcination temperatures were utilized, whereas in series II, molar ratios of nitric acid to hydrochloric acid were employed.

Series I: Synthesis of titania particles was achieved utilizing titanium isopropoxide (Ti i(PrO)$_4$) as the precursor. This precursor was incrementally introduced, via a dropwise method, into diverse solutions of nitric acid (HNO_3), accompanied by continuous stirring for a duration of 30 minutes at ambient temperature. To one synthesis batch, sodium fluoride (NaF) was incorporated to evaluate its effect, given that the fluoride ion (F^-) demonstrates a pronounced complexation propensity towards Ti(IV). The specific compositions for each solution are enumerated in Table No. 1.

After the completion of the stirring phase, all synthetic mixtures were transferred to hermetically sealed polyethylene containers and subjected to an aging process at 85°C within an oven for a period of 24 hours. Post-aging, selected sample aliquots underwent calcination at temperatures of 300°C and 500°C. The residual precipitates were subjected to centrifugation at 8000 rpm for 10 minutes followed by washing. The precipitates that resulted from this process were then calcined at a temperature of 300°C.

Box 1

Table 1

Reactant Concentrations for Titanium Dioxide Synthesis in Series I

Reactant	Sample				
	I-1	I-2	I-3	I-4	I-5
HNO_3	0M	1M	3M	1M	0.5M
Ti i(PrO)$_4$	0.15M	0.15M	0.15M	0.15M	0.15M
NaF	-	-	-	0.01M	-

Source: own elaboration

ISSN: 2523-6784.
RENIECYT-CONAHCYT: 1702902

Del Ángel-Sánchez, María Magdalena & Martínez-Carreón, María de Jesús. [2024]. Influence of concentration, acid type and calcination temperature on TiO_2 synthesis. Journal of Systematic Innovation. 8[22]1-11: e4822111.
https://doi.org/10.35429/JSI.2024.8.22.1.11

Series II: Titanium dioxide was synthesized by introducing titanium isopropoxide into a variety of HCl and HNO_3 solutions, maintaining an aggregate acid concentration of 3M while varying their respective proportions. The synthesis proceeded under continuous stirring for 30 minutes. The final concentrations are enumerated in Table No. 2.

Subsequently, the samples underwent an aging process for 24 hours at 85°C within a controlled oven environment. Post-aging, the samples were subjected to centrifugation, and the resultant solid was rinsed and re-centrifuged at 8000 rpm for a duration of 5 minutes. The solid isolated from this stage was then redissolved in 50 mL of 3M HNO_3 with stirring maintained for 20 minutes. Following this, the samples were once again centrifuged and washed; the solid fraction was segregated from the supernatant and subsequently desiccated.

Box 2

Table 2

Reactant Concentrations for Titanium Dioxide Synthesis in Series II

Reactant	Sample		
	II-1	II-2	II-3
HNO_3	0.5M	1M	1.5M
HCl	2.5M	2M	1.5M
Ti i$(PrO)_4$	0.15M	0.15M	0.15M

The suspensions derived post-centrifugation in series I were subjected to particle size analysis utilizing a Dynamic Light Scattering (DLS) device NanoBrook 90Plus Particle Size Analyzer (Brookhaven Instruments Corporation).

The two series of samples were characterized by XRD using a PANalytical X'Pert PRO diffractometer operated at 40kV and 40mA, employing Cu-Kα radiation (λ= 1.54060Å) with a step size of 0.0260° and a counting time of 1.0s per step.

The presence of functional groups was determined using a Shimadzu IRAffinity FTIR instrument, equipped with a Gladi ATR module (PIKE Technologies, INC) with a spectral range of 500 to 4000 cm^{-1}.

The morphology of the materials was determined using Field Emission Scanning Electron Microscopy (FESEM) on a Carl Zeiss Supra 40 NTS instrument.

Results and discussions

Characterization by DLS

The soles obtained from samples I-2, I-4, and I-5 were characterized. Samples I-1 and I-3 could not be peptized due to consecutive washing of the solid obtained by thermal hydrolysis.

Figures 1 to 3 display the histograms corresponding to the different samples. In sample I-2, a particle size of 220 nm with a polydispersity index of 0.261 was obtained, sample I-4 has a particle size of 167 nm with a polydispersity index of 0.278, while in sample I-5, the particle size is 1291 nm with a polydispersity index of 0.005. In syntheses I-2 and I-4, higher acid concentrations were used compared with sample I-5, which generated smaller particles resulting in a more stable sol. Sample I-5, containing a lower concentration of HNO_3, produced an unstable sol that formed a precipitate after 30 minutes.

Box 3

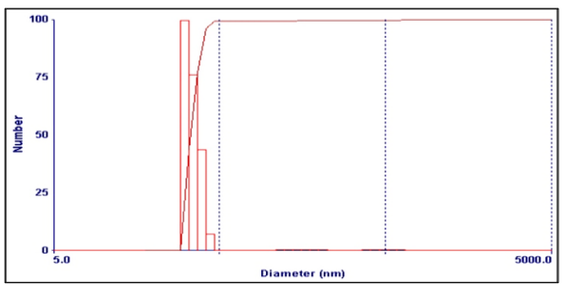

Figure 1

DLS size distribution of sample I-2

Source: 90Plus Nanoparticle Size Analyzer

Box 4

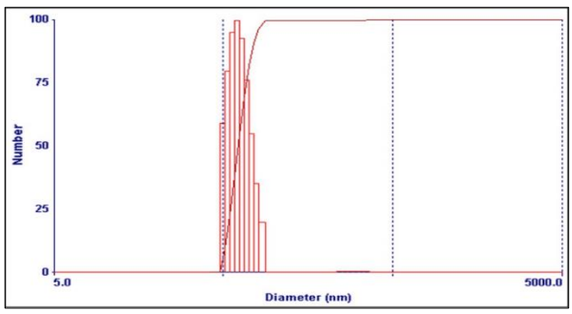

Figure 2

DLS size distribution of sample I-4

Source: 90Plus Nanoparticle Size Analyzer

ISSN: 2523-6784.
RENIECYT-CONAHCYT: 1702902

Del Ángel-Sánchez, María Magdalena & Martínez-Carreón, María de Jesús. [2024]. Influence of concentration, acid type and calcination temperature on TiO_2 synthesis. Journal of Systematic Innovation. 8[22]1-11: e4822111.
https://doi.org/10.35429/JSI.2024.8.22.1.11

Box 5

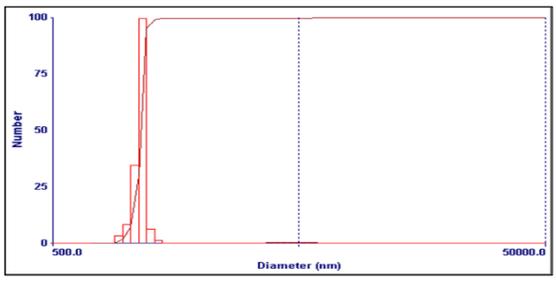

Figure 3

DLS size distribution of sample I-5

Source: 90Plus Nanoparticle Size Analyzer

Characterization by XRD

The samples from series I, subjected to calcination at 300°C, were analyzed using X-ray diffraction (XRD). In Figure 4, it is evident that samples I-2 and I-5 exhibit the crystalline phase of anatase, as indicated by the International Centre for Diffraction Data (ICDD) card 00-004-0477. Conversely, the crystalline phase of sample I-3 corresponds to rutile, matching with the information linked to the ICDD 01-073-1765 card.

Box 6

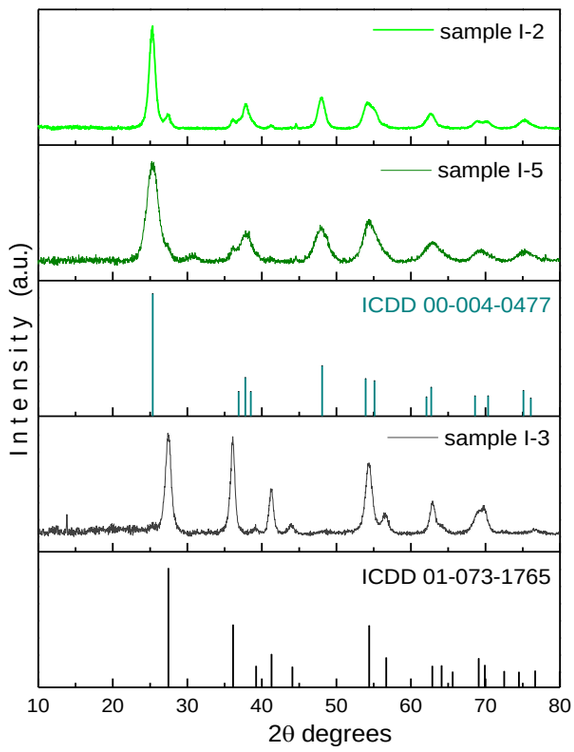

Figure 4

X-ray diffraction patterns of Series I samples calcined at 300°C

Source: Own elaboration

The average crystallite sizes of the samples presented in Table 3 were determined using the Scherrer equation, analyzing the diffraction peaks with the X'Pert HighScore Plus software.

Box 7

Table 3

Crystallite Size of Series I Samples Calcined at 300°

Sample	Crystallite size [Å]
I-2	81.5
I-3	108.2
I-5	41.6

Source: own elaboration

XRD analysis was performed on Series I samples calcined at 500°C. The corresponding diffractograms are presented in Figure 5. Consistent with the observations for samples calcined at 300°C, samples I-2 and I-5 exhibit the anatase crystalline phase, as evidenced by their diffraction patterns matching the ICDD card 00-004-0477. In contrast, sample I-3 possesses a rutile crystalline phase, as confirmed by its diffraction pattern aligning with the ICDD card 01-073-1765.

Box 8

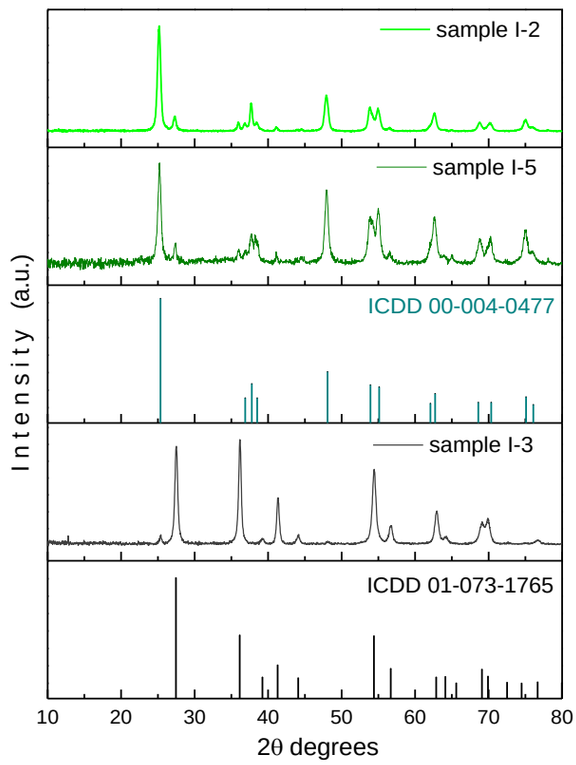

Figure 5

X-ray diffraction patterns of Series I samples calcined at 500°C

Source: Own elaboration

ISSN: 2523-6784.
RENIECYT-CONAHCYT: 1702902

Del Ángel-Sánchez, María Magdalena & Martínez-Carreón, María de Jesús. [2024]. Influence of concentration, acid type and calcination temperature on TiO_2 synthesis. Journal of Systematic Innovation. 8[22]1-11: e4822111.
https://doi.org/10.35429/JSI.2024.8.22.1.11

Crystallite size was determined by analyzing the diffraction peaks of Figure 5 using the Scherrer equation within X'Pert HighScore Plus software. The results are presented in Table 4.

Box 9

Table 4

Crystallite Size of Series I Samples Calcined at 500°

Sample	Crystallite size [Å]
I-2	170.9
I-3	182.5
I-5	161.5

Source: own elaboration

In the syntheses of Series I, it is evident that as the precursor solution is prepared in a more acidic medium, the development of the rutile phase is favored (sample I-3), in contrast to samples synthesized in a less acidic medium (samples I-2 and I-5), where characteristic peaks corresponding to the anatase phase are observed.

Regarding the calcination temperature, examination of the diffractograms in figures 4 and 5 reveals that there is no change in the samples with respect to the phases present. However, the thermal treatment led to an increase in crystal size, as evident in Tables 3 and 4.

The average crystallite sizes of the Series II samples depicted in Table 5 were obtained through the Scherrer equation, utilizing an analysis of the diffraction peaks of Figure 6 with the X'Pert HighScore Plus software.

Box 10

Table 5

Crystallite Size Analysis of Series II Samples

Sample	Crystallite size [Å]
II-1	98.8
II-1	84.5
II-1	650.5

Source: own elaboration

Figure 6 presents the diffractograms corresponding to the various samples from Series II. Notably, when the precursor solution employed a 1:1 ratio of HNO_3 to HCl (sample II-3), titanium oxide oxalate hydroxide hydrate was obtained, consistent with the crystallographic data from ICDD 00-048-1164.

In contrast, for other ratios, only the rutile phase was identified, as indicated by the crystallographic card ICDD 01-073-1765.

Box 11

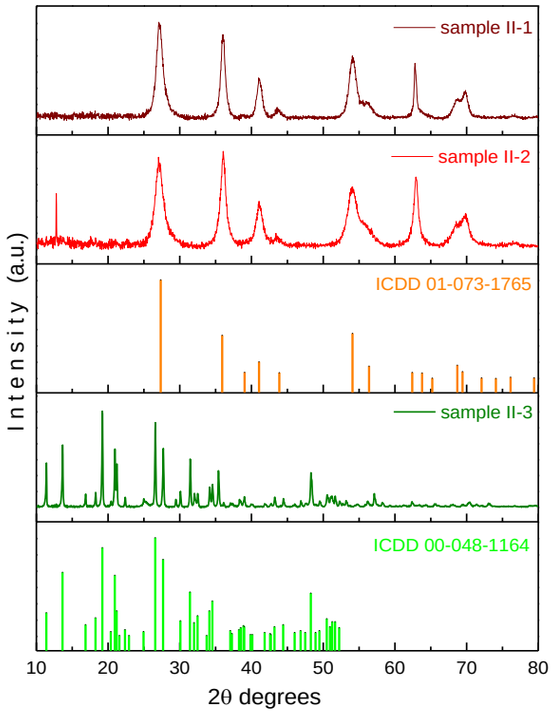

Figure 6

X-ray diffraction patterns of Series II

Source: Own elaboration

Characterization by ATR-FTIR

The functional groups present in the samples were identified by ATR-FTIR spectroscopy.

The FTIR transmission spectrum of Series I samples, calcined at 300°C and 500°C, is shown in Figure 7. Notably, the spectrum reveals the presence of broad bands associated with hydroxyl groups (O–H stretching vibration) in the 3000 cm^{-1} – 3600 cm^{-1} range. Specifically, for sample I-1, synthesized without HNO_3, the corresponding peak related to this OH group is notably small.

Additionally, a band around 1650 cm^{-1} is attributed to absorbed water molecules (H–O–H symmetric vibration) on the surface of the TiO_2 crystal (Sanchez-Martinez, 2019). Furthermore, the broad band spanning the 1000 cm^{-1} to 400 cm^{-1} region is ascribed to Ti-O stretching and Ti-O-Ti bridging stretching modes (Praveen, 2014).

ISSN: 2523-6784.
RENIECYT-CONAHCYT: 1702902

Del Ángel-Sánchez, María Magdalena & Martínez-Carreón, María de Jesús. [2024]. Influence of concentration, acid type and calcination temperature on TiO_2 synthesis. Journal of Systematic Innovation. 8[22]1-11: e4822111.
https://doi.org/10.35429/JSI.2024.8.22.1.11

Box 12

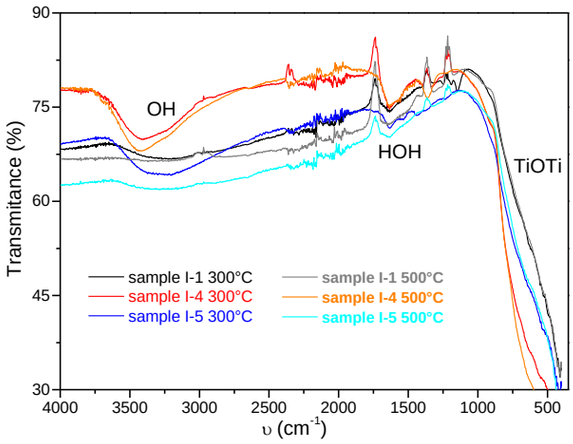

Figure 7

ATR-FTIR spectra of Series I samples

Source: Own elaboration

The ATR-FTIR spectra of Series II samples, observed on Figure 8, exhibit several distinct absorption bands that can be attributed to the various vibrational modes of the oxalate and titanium-oxygen bonding. For instance, the band in the 3000 cm^{-1} – 3600 cm^{-1} range is associated with hydroxyl groups (O–H stretching vibration) (Sanchez-Martinez, 2019), a band in the region of 2300-2400 cm^{-1} is frequently observed and is attributed to the adsorption of atmospheric CO_2 on the sample surface during the measurement (Liu, 2014), the strong absorption bands observed in the 1600-1700 cm^{-1} region on sample II-3 are characteristic of the C=O stretching vibrations of the oxalate group (Young, 2009) while to samples II-1 and II-2 this band is associated with the NO-stretching (Nishikiori, 2011), the band at around 900 cm^{-1} is associated to the Ti-O-Ti vibrations (Haggerty et al., 2017) and the band that appears around 800 cm^{-1} range are associated with the Ti-O stretching vibrations (Liu, 2014).

Box 13

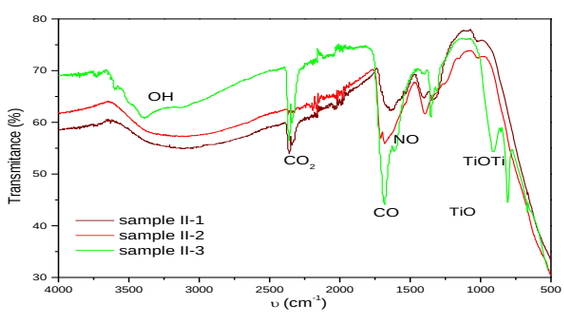

Figure 8

ATR-FTIR spectra of Series II samples

Source: own elaboration

ISSN: 2523-6784.
RENIECYT-CONAHCYT: 1702902

Characterization by SEM

Scanning Electron Microscopy (SEM) images provides detailed insights into the morphology and structure of materials. In Series I, Figures 9 to 18 display a scale bar on the left side, indicating 1 micron, emphasizing the high magnification level. On the right side, these figures zoom in further, revealing finer details with a 20 nm scale bar. For Series II, Figures 19 to 21 show a scale bar on the upper side, also indicating 1 micron, highlighting the high magnification level. The lower side of these figures provides even closer views, displaying finer details with a 200 or 100 nm scale bar.

Box 14

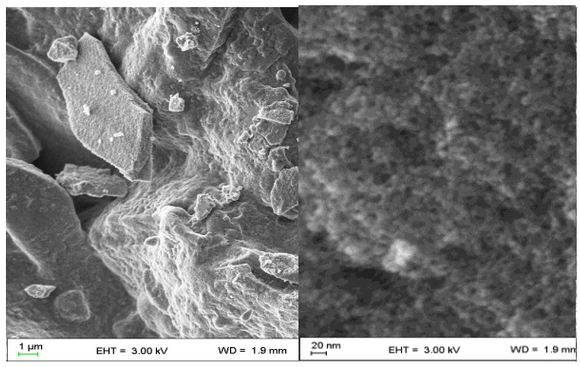

Figure 9

SEM micrograph of Sample I-1 calcinated at 300ºC

Source: Carl Zeiss Supra 40

Box 15

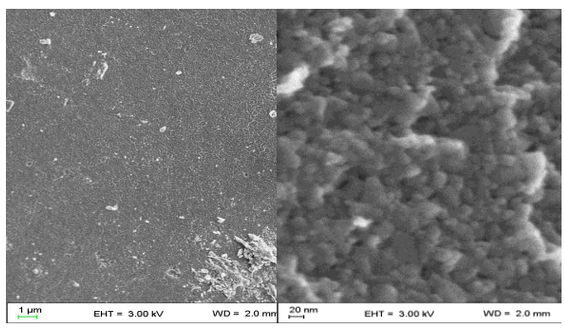

Figure 10

Sample I-1 calcinated at 500ºC

Source: Carl Zeiss Supra 40

Figure 9 shows the morphology of sample I-1 calcinated at 300°C. At this temperature, various structures are visible, including flat, angular plate-like formations and fibrous patterns on surface texture, the particle size appears to be in the nanometer range, and there is minimal evidence of agglomeration. The overall structure is porous, which is typical for TiO2 calcinated at lower temperatures.

In contrast, the SEM image in Figure 10 of the sample calcinated at 500°C shows that particles are larger and more crystalline compared to those in Figures 9, there is a noticeable increase in particle size, and the surface texture appears relatively smooth, with occasional roughness. Additionally, there is evidence of particle sintering, leading to a denser structure with reduced porosity.

Box 16

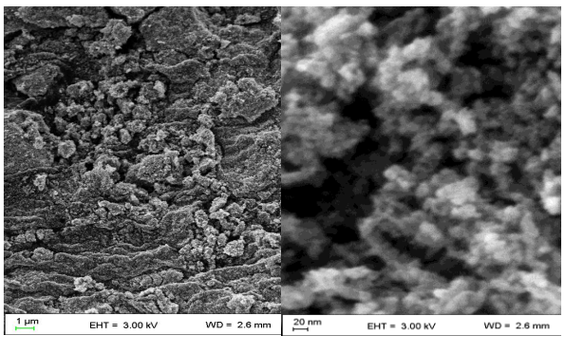

Figure 11

Sample I-2 calcinated at 300ºC

Source: Carl Zeiss Supra 40

Box 17

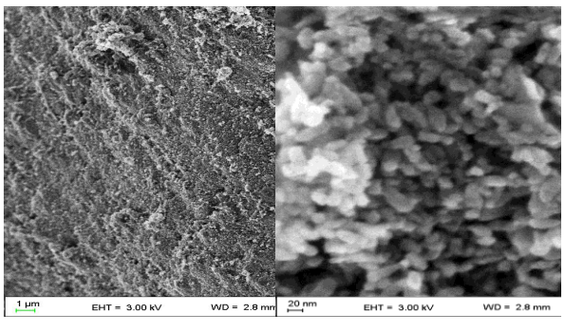

Figure 12

Sample I-2 calcinated at 500ºC

Source: Carl Zeiss Supra 40

The SEM image of sample I-2 calcinated at 300°C shown on Figure 11, appears more irregular and porous compared to the same sample calcined at 500°C (Figure 12) which exhibits a more uniform and crystalline structure.

This suggests that higher calcination temperature have improved the crystallinity and reduced the surface defects of the nanoparticles, the differences in morphology are attributed to the increased thermal energy promoting the elimination of surface defects, leading to a more ordered and crystalline structure.

Box 18

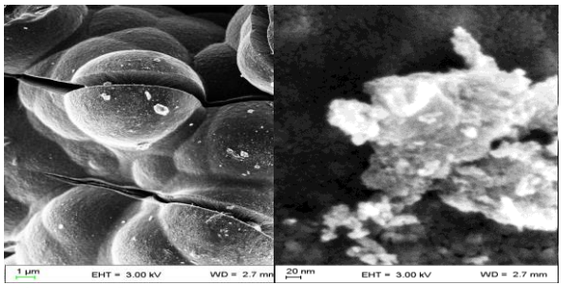

Figure 13

Sample I-3 calcinated at 300ºC

Source: Carl Zeiss Supra 40

Box 19

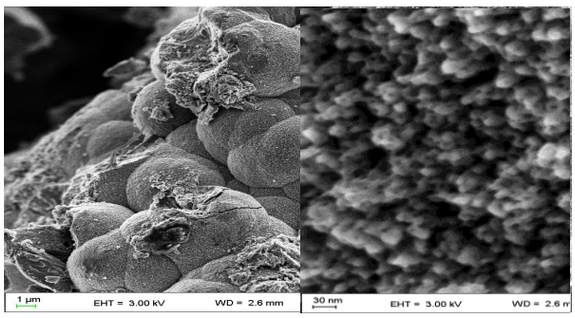

Figure 14

Sample I-3 calcinated at 500ºC

Source: Carl Zeiss Supra 40

For sample I-3, Figure 13, calcinated at 300°C exhibiting a more porous and fibrous structure compared to Figure 14 related to the sample calcinated at 500°C, which displayed a denser and more crystalline appearance. This change in morphology was attributed to the increased thermal energy imparted to the TiO_2 particles during the higher temperature calcination process. The higher thermal energy input also affected the particle size distribution, with the 500°C calcined sample displaying a narrower and more finely dispersed particle size distribution compared to the 300°C calcined sample.

Box 20

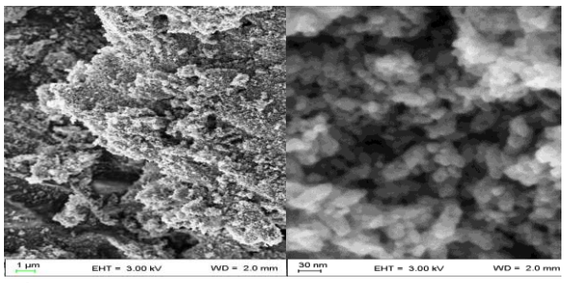

Figure 15

Sample I-4 calcinated at 300ºC

Source: Carl Zeiss Supra 40

ISSN: 2523-6784.
RENIECYT-CONAHCYT: 1702902

Del Ángel-Sánchez, María Magdalena & Martínez-Carreón, María de Jesús. [2024]. Influence of concentration, acid type and calcination temperature on TiO_2 synthesis. Journal of Systematic Innovation. 8[22]1-11: e4822111.
https://doi.org/10.35429/JSI.2024.8.22.1.11

Box 21

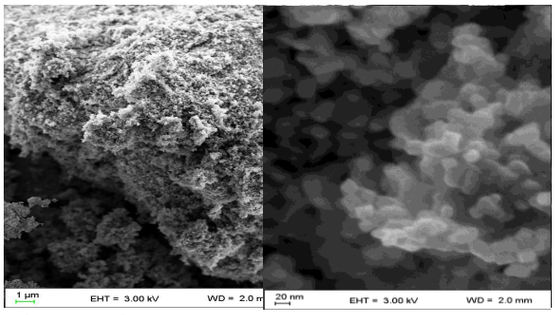

Figure 16

Sample I-4 calcinated at 500ºC

Source: Carl Zeiss Supra 40

SEM micrograph of sample I-4 calcinated at 300°C are displayed on Figure 15 and Figure 16 corresponds to the same sample calcinated at 500°C. It is observed that the micrographs show change in crystal structure and surface morphology after calcination at 500°C compared to 300°C. The surface morphology of image calcinated at 300°cindicates a relatively rough and porous nature with irregularly shaped particles, whereas the surface morphology of image calcinated at 500°C exhibits a much smoother and more uniform surface with smaller and more rounded particles.

Box 22

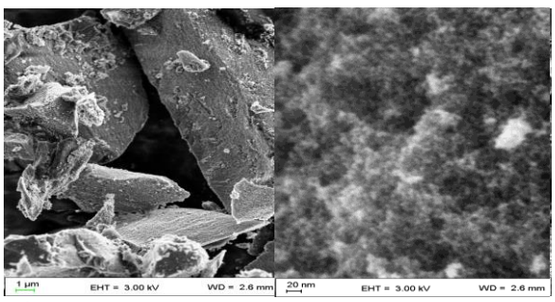

Figure 17

Sample I-5 calcinated at 300ºC

Source: Carl Zeiss Supra 40

Box 23

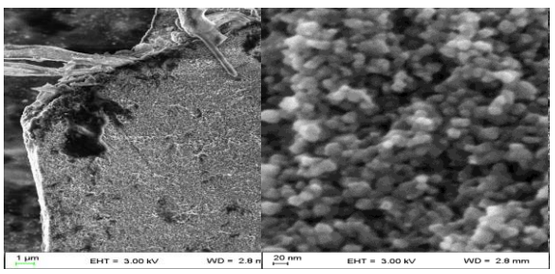

Figure 18

Sample I-5 calcinated at 500ºC

Source: Carl Zeiss Supra 40

The differences observed in the SEM images of sample I-5 can be attributed to the impact of calcination temperature on the crystallization and phase transformation. The lower calcination temperature of 300°C was not sufficient to fully promote the crystallization of TiO_2, leading to the formation of larger, more irregular, and fibrous particles like is observed on Figure 17, this is likely due to the incomplete phase transformation from the amorphous to the crystalline phase. In contrast, Figure 18 indicates that the higher calcination temperature of 500°C enabled the complete crystallization of the material. This resulted in the formation of smaller, more uniform, and spherical particles with a relatively smooth surface morphology. The elevated temperature facilitated improved atomic rearrangement and the growth of well-defined titania crystal structures.

SEM images in Figures 19 to 21 depict the titania synthesis process using varying ratios of nitric acid (HNO_3) to hydrochloric acid (HCl).

Box 24

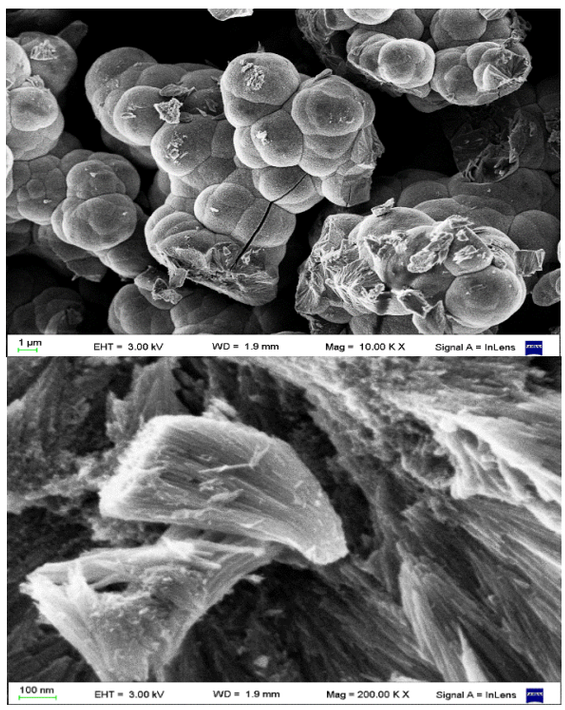

Figure 19

Sample II-1, obtained with a 1:5 ratio of HNO_3 to HCl

Source: Carl Zeiss Supra 40

ISSN: 2523-6784.
RENIECYT-CONAHCYT: 1702902

Del Ángel-Sánchez, María Magdalena & Martínez-Carreón, María de Jesús. [2024]. Influence of concentration, acid type and calcination temperature on TiO_2 synthesis. Journal of Systematic Innovation. 8[22]1-11: e4822111.
https://doi.org/10.35429/JSI.2024.8.22.1.11

Box 25

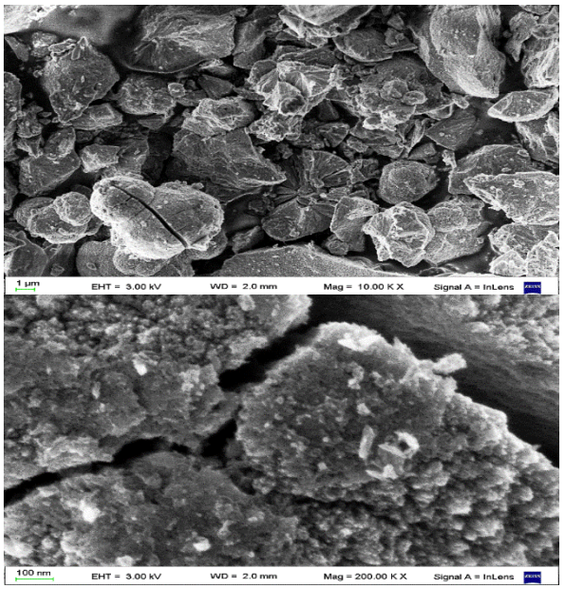

Figure 20

Sample II-2, obtained with a 1:2 ratio of HNO_3 to HCl

Source: Carl Zeiss Supra 40

Figure 19 corresponds to the product obtained with a 1:5 HNO_3-to-HCl ratio, Figure 20 with a 1:2 ratio, and Figure 21 with a 1:1 ratio. Figures 19 and 20 indeed reveal similar particle morphology, characterized by spherical shapes. The confirmation through X-ray diffraction (XRD) analysis further supports the presence of the rutile phase of titanium dioxide in these samples.

Box 26

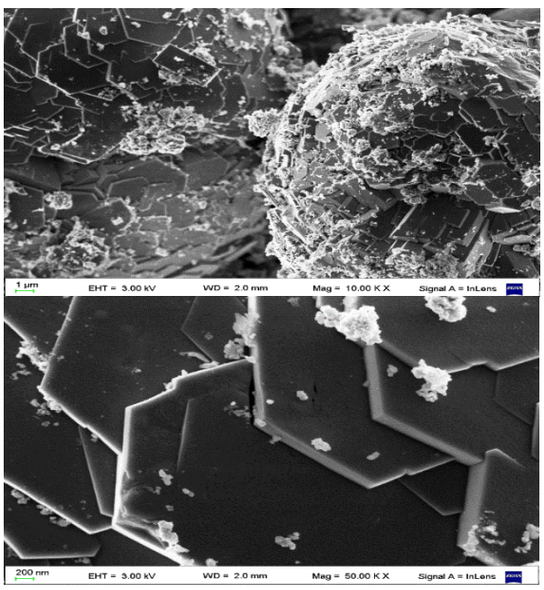

Figure 21

Sample II-3, obtained with a 1:1 ratio of HNO_3 to HCl

Source: Carl Zeiss Supra 40

However, Figure 21 represents a distinct scenario, the synthesis of titanium oxalate. The particles in this case exhibit hexagonal shapes, indicating a different crystal structure and morphology compared to the rutile phase observed in figures 19 and 20.

The impact of the HNO_3-to-HCl ratio on the final product on the crystalline phase has significantly influences. In the case of rutile, the 1:5 and 1:2 ratios (Figures 19 and 20) favor its formation. However, the 1:1 ratio (Figure 21) leads to the synthesis of titanium oxalate. The specific acid concentrations affect the availability of precursor ions and their interactions during nucleation and growth When considering particle size and shape, smaller acid ratios may promote nucleation and result in smaller particles, while larger ratios may lead to larger particles. The spherical morphology observed in rutile (Figures 19 and 20) suggests controlled growth under specific conditions. The hexagonal shapes in titanium oxalate (Figure 21) indicate different growth mechanisms. Beyond individual particles, the overall morphology of the synthesized material is influenced. The arrangement of particles, agglomeration, and surface features contribute to the macroscopic appearance. The distinct hexagonal coverage in Figure 21 highlights the unique morphology of titanium oxalate.

Conclusions

In Series 1, it was observed that higher nitric acid concentrations predominantly favor the development of the rutile phase, while lower concentrations lead to the formation of the anatase phase. Intermediate acid concentrations result in more stable sols. Furthermore, the pronounced aggregation and rougher surface of the particles calcined at 300°C suggest that the lower calcination temperature was not sufficient to overcome the attractive forces between the particles, leading to the formation of larger agglomerates. In comparison, the higher temperature of 500°C enabled better control over the particle growth, resulting in a more uniform and less aggregated particle distribution. Notably, the type and concentration of acid exert a more significant influence on phase determination than thermal treatment. Additionally, the presence of fluoride induces a slight increase in nanoparticle size.

ISSN: 2523-6784.
RENIECYT-CONAHCYT: 1702902

Del Ángel-Sánchez, María Magdalena & Martínez-Carreón, María de Jesús. [2024]. Influence of concentration, acid type and calcination temperature on TiO_2 synthesis. Journal of Systematic Innovation. 8[22]1-11: e4822111.
https://doi.org/10.35429/JSI.2024.8.22.1.11

In Series 2, it was determined that a higher proportion of hydrochloric acid (HCl) compared to nitric acid (HNO_3) induces the formation of the rutile phase of TiO_2. Conversely, when the acid ratio is equal, that is, a 1:1 proportion, the generation of Titanium oxide oxalate hydroxide hydrate is favored.

These findings underscore the significance of acid composition in hydrothermal synthesis and its direct influence on the crystalline phase, particle size and shape and overall morphology of the synthesized titanium-based materials.

Declarations

Conflict of interest

The authors hereby declare that there are no conflicts of interest associated with this publication

Authors' Contributions

All authors have made equal and significant contributions to the development and completion of this research paper. Each author has been actively involved in the conceptualization, experimental analysis, and interpretation of the research findings.

Availability of data and materials

All data generated or analyzed during this study are included in this published manuscript

Financing

This work has been funded by CONAHCYT through the postdoctoral grant [BP-PA-2022070515071574 8-2482439]

Acknowledgements

The authors would like to thank the Laboratory of Nanosciences and Nanotechnology of the Universidad Autónoma de Nuevo León for their assistance.

Abbreviations

ATR-FTIR	Attenuated Total Reflectance Fourier Transform Infrared Spectroscopy
DLS	Dynamic Light Scattering
FESEM	Field Emission Scanning Electron Data Microscopy
HCl	Hydrochloric acid
HNO_3	Nitric acid
ICDD	The International Centre for Diffraction
MOCVD	X-Ray Diffraction
NaF	metal-organic chemical vapor deposition
SEM	Sodium fluoride
Ti i(PrO)$_4$	Scanning Electron Microscopy
TiO_2	Titanium isopropoxide
XRD	Titanium Dioxide
	X-ray diffraction

References

Background

Ali, I., Suhail, M., Alothman, Z. A., & Alwarthan, A. (2018). Recent advances in syntheses, properties and applications of TiO2 nanostructures. RSC Advances, 8(53), 30125–30147.

Background

Anandgaonker, P., Kulkarni, G., Gaikwad, S., & Rajbhoj, A. (2019). Synthesis of TiO2 nanoparticles by electrochemical method and their antibacterial application. Arabian Journal of Chemistry, 12(8), 1815–1822.

Arun, J., Nachiappan, S., Rangarajan, G., Alagappan, R. P., Gopinath, K. P., & Lichtfouse, E. (2023). Synthesis and application of titanium dioxide photocatalysis for energy, decontamination and viral disinfection: a review. Environmental Chemistry Letters, 21(1), 339–362.

Dülger, B., Özkan, G., Angı, O. S., & Özkan, G. (2024). Green synthesis of TiO2 nanoparticles using Aloe Vera extract as catalyst support material and studies of their catalytic activity in dehydrogenation of Ethylenediamine Bisborane. International Journal of Hydrogen Energy.

ISSN: 2523-6784.
RENIECYT-CONAHCYT: 1702902

Farooq, N., Kallem, P., ur Rehman, Z., Imran Khan, M., Kumar Gupta, R., Tahseen, T., Mushtaq, Z., Ejaz, N., & Shanableh, A. (2024). Recent trends of titania (TiO_2) based materials: A review on synthetic approaches and potential applications. Journal of King Saud University. Science, 36(6), 103210.

Guo, J., Zhu, S., Chen, Z., Li, Y., Yu, Z., Liu, Q., Li, J., Feng, C., & Zhang, D. (2011). Sonochemical synthesis of TiO2 nanoparticles on graphene for use as photocatalyst. Ultrasonics Sonochemistry, 18(5), 1082–1090.

Hidalgo, M. C., Aguilar, M., Maicu, M., Navío, J. A., & Colón, G. (2007). Hydrothermal preparation of highly photoactive TiO2 nanoparticles. Catalysis Today, 129(1–2), 50–58.

Li, W., Ismat Shah, S., Huang, C.-P., Jung, O., & Ni, C. (2002). Metallorganic chemical vapor deposition and characterization of TiO2 nanoparticles. Materials Science & Engineering. B, Solid-State Materials for Advanced Technology, 96(3), 247–253.

Pelaez, M., Nolan, N. T., Pillai, S. C., Seery, M. K., Falaras, P., Kontos, A. G., Dunlop, P. S. M., Hamilton, J. W. J., Byrne, J. A., O'Shea, K., Entezari, M. H., & Dionysiou, D. D. (2012). A review on the visible light active titanium dioxide photocatalysts for environmental applications. Applied Catalysis. B, Environmental, 125, 331–349.

Basics

Bindra, P., Mittal, H., Sarkar, B. R., & Hazra, A. (2022). Synthesis of highly ordered TiO2 nanorods on a titanium substrate using an optimized hydrothermal method. Journal of Electronic Materials, 51(4), 1707–1716.

Eaimsumang, S., Prataksanon, P., Pongstabodee, S., & Luengnaruemitchai, A. (2020). Effect of acid on the crystalline phase of TiO2 prepared by hydrothermal treatment and its application in the oxidative steam reforming of methanol. Research on Chemical Intermediates, 46(2), 1235–1254.

Gupta, T., Samriti, Cho, J., & Prakash, J. (2021). Hydrothermal synthesis of TiO2 nanorods: formation chemistry, growth mechanism, and tailoring of surface properties for photocatalytic activities. Materials Today. Chemistry, 20(100428), 100428.

Kignelman, G., & Thielemans, W. (2021). Meta-analysis of TiO2 nanoparticle synthesis strategies to assess the impact of key reaction parameters on their crystallinity. Journal of Materials Science, 56(10), 5975–5994.

Rehan, M., Lai, X., & Kale, G. M. (2011). Hydrothermal synthesis of titanium dioxide nanoparticles studied employing in situ energy dispersive X-ray diffraction. CrystEngComm, 13(11), 3725.

Support

Haggerty, J. E. S., Schelhas, L. T., Kitchaev, D. A., Mangum, J. S., Garten, L. M., Sun, W., Stone, K. H., Perkins, J. D., Toney, M. F., Ceder, G., Ginley, D. S., Gorman, B. P., & Tate, J. (2017). High-fraction brookite films from amorphous precursors. Scientific Reports, 7(1), 1–11.

Liu, C., Zhang, D., & Sun, Y. (2014). Synthesis of hollow anatase spheres with enhanced optical performance. CrystEngComm, 16(36), 8421.

Nishikiori, H., Fukasawa, Y., Yokosuka, Y., & Fujii, T. (2011). Nitrogen doping into titanium dioxide by the sol–gel method using nitric acid. Research on Chemical Intermediates, 37(8), 869–881.

Sanchez-Martinez, A., Koop-Santa, C., Ceballos-Sanchez, O., López-Mena, E. R., González, M. A., Rangel-Cobián, V., Orozco-Guareño, E., & García-Guaderrama, M. (2019). Study of the preparation of TiO2 powder by different synthesis methods. Materials Research Express, 6(8), 085085.

Praveen, P., Viruthagiri, G., Mugundan, S., & Shanmugam, N. (2014). Structural, optical and morphological analyses of pristine titanium di-oxide nanoparticles – Synthesized via sol–gel route. Spectrochimica Acta. Part A, Molecular and Biomolecular Spectroscopy, 117, 622-629.

ISSN: 2523-6784.
RENIECYT-CONAHCYT: 1702902

Del Ángel-Sánchez, María Magdalena & Martínez-Carreón, María de Jesús. [2024]. Influence of concentration, acid type and calcination temperature on TiO_2 synthesis. Journal of Systematic Innovation. 8[22]1-11: e4822111.
https://doi.org/10.35429/JSI.2024.8.22.1.11